



## Article

# Stability Analysis of Rocky Slopes on the Cuenca–Girón–Pasaje Road, Combining Limit Equilibrium Methods, Kinematics, Empirical Methods, and Photogrammetry

Xavier Delgado-Reivan <sup>1</sup>, Cristhian Paredes-Miranda <sup>1</sup>, Silvia Loaiza <sup>1</sup> , Michelle Del Pilar Villalta Echeverria <sup>1</sup>, Maurizio Mulas <sup>1,\*</sup> and Luis Jordá-Bordehore <sup>2</sup>

<sup>1</sup> Faculty of Engineering in Earth Sciences (FICT), ESPOL Polytechnic University, Gustavo Galindo Campus Km 30.5 Perimetral, Guayaquil P.O. Box 09-01-5863, Ecuador

<sup>2</sup> Department of Engineering and Terrain Morphology, Polytechnic University of Madrid, 28040 Madrid, Spain

\* Correspondence: mmulas@espol.edu.ec; Tel.: +593-998-250-529

**Abstract:** The 3D point clouds obtained from the low-cost, remote, and precise SfM (Structure from Motion) technique allow the extraction and acquisition of discontinuities and their characteristics both manually, with the compass and virtual ruler of the Cloud Compare software, and automatically with the DSE (Discontinuity Set Extractor) program, which is faster, more accurate, and safe. Some control plans have been used, which basically consist of identifying one or several fractures and taking measurements on them manually and remotely. The difference between both types of measurements is around 5°, which we believe is reasonable since it is within the precision and repeatability of measurements with a geologist's compass. This work analyzes the stability of six slopes (five excavated and one natural) by applying five different analysis methodologies based on the rock mass classification system (SMR, RHRSmod, and Qslope), kinematic analysis, and analytical analysis (limit equilibrium). Their results were compared with what was observed in the field to identify the most appropriate analysis methodologies adjusted to reality. The necessary parameters for analyzing each of the slopes, such as orientation, quantity, spacing, and persistence of the discontinuities, were obtained from the automatic analysis. This type of analysis eliminates the subjectivity of the authors, although the findings are related and resemble those obtained manually. The main contribution of the article consists of the application of fast and low-cost techniques to the evaluation of slopes. It is a type of analysis that is in high demand today in many Andean countries, and this work aims to provide an answer. These methodologies suggested by scientific articles such as this one will later be integrated into some procedures and will be taken into account by technical reports. The results show that with the available information and by applying low-cost techniques, the SMR system is the methodology that presents the best results and adjusts better to the reality of the study area. Therefore, SMR is a necessary parameter to determine rockfall hazards through modified RHRS.

**Keywords:** structure from motion; discontinuity set extractor; cloud compare; rock mass classification; analytical analysis; kinematic analysis



**Citation:** Delgado-Reivan, X.; Paredes-Miranda, C.; Loaiza, S.; Echeverria, M.D.P.V.; Mulas, M.; Jordá-Bordehore, L. Stability Analysis of Rocky Slopes on the Cuenca–Girón–Pasaje Road, Combining Limit Equilibrium Methods, Kinematics, Empirical Methods, and Photogrammetry. *Remote Sens.* **2023**, *15*, 862. <https://doi.org/10.3390/rs15030862>

Academic Editor: Radosław Juszczak

Received: 23 November 2022

Revised: 30 January 2023

Accepted: 31 January 2023

Published: 3 February 2023



**Copyright:** © 2023 by the authors. Licensee MDPI, Basel, Switzerland. This article is an open access article distributed under the terms and conditions of the Creative Commons Attribution (CC BY) license (<https://creativecommons.org/licenses/by/4.0/>).

## 1. Introduction

Characterizing the rock mass and analyzing the stability of rocky slopes on roads is fundamental and necessary to guarantee users' safety. Slope analysis is traditionally carried out using geomechanical stations with a hand compass, tape measure, and other tools to describe the conditions of the joints, such as the sclerometer and Barton comb [1]. There are several methodologies for slope stability analysis: limit equilibrium methods [2–4]; kinematic analysis [5,6]; empirical methods, such as geomechanical classifications (Rock Mass Classification—RMR; Barton's Q Index— $Q_{system}$ ; Barton's Q Slope Index— $Q_{slope}$ ; Slope Mass Classification—SMR; Rockfall Hazard Classification System—RHRS) [7–9]; numerical methods [10,11]. All these methodologies need a correct characterization of the

discontinuities since the mechanical, hydraulic, and deformational behavior of the rock mass depends on them [12]. Discontinuities are nothing more than cracks and fractures in the rock mass with low or no tensile strength [13].

The analysis of discontinuities in rocky slopes through 3D point clouds (3DPC), obtained through remote techniques such as Structure from Motion (SfM), has been gaining prominence in recent years. SfM provides geometric information on the external surface of the slope, allowing the obtaining of data in places of difficult access and their safe analysis. With the SfM technique, high-resolution data sets are identified at different scales and at a low cost, requiring only superimposed and displaced images [14], which makes it ideal for low-cost research in remote areas, as the case of this study. In addition, by SfM, the recognition and classification of discontinuities through semi-automatic recognition methodologies can be possible [15–18]. Various algorithms developed in recent years [16,19–21] allow the automatic acquisition of the discontinuity planes (spacing, persistence, roughness) from 3DPC of physical parameters. The level of detail obtained in 3DPC with SfM techniques, according to [12], is similar to that obtained by laser scanning techniques, with the great advantage of being a considerably cheaper technique. On the other hand, [22] considers acceptable a difference in orientation values of the discontinuities measured in the field with a 3DPC of  $\pm 5^\circ$ . In the slopes analyzed in the present study, there is an average precision of  $4^\circ$  for the direction of the dip and  $2^\circ$  for the dip, with a maximum variability of  $6^\circ$  in the direction of the dip in one of the slopes studied. Similarly, [22] point out that the automatic extraction of discontinuities can be considered the most objective method since it minimizes the operator's influence. Therefore, for the stability analysis carried out in this study, we worked with the information obtained automatically using the Discontinuity Set Extractor (DSE) algorithm.

The general objective of this study is to assess the benefits of each of the different slope stability analysis methodologies based on the data obtained from the 3DPC to identify the method that best fits the reality of the study area. To this end, slope stability analysis with empirical methods SMR,  $Q_{\text{slope}}$ , and  $RHRS_{\text{mod}}$  [8,23,24], the limit equilibrium method with the help of commercial programs such as Rocplane and Swedge from Rocscience (limit equilibrium analysis is not performed for overturning failures because the detailed geometry of the slopes is not available), and finally kinematic analysis applying the JRC-JCS model by Barton and Bandis detailed in [25] are proposed.

The study area is located to the South West of the Ecuadorian Andes (Figure 1a), specifically between km 78 + 000–92 + 000 of the Cuenca–Girón–Pasaje road heading East–West (Figure 1b). The sector is mainly made up of ignimbritic deposits belonging to the Saraguro Group and the Jubones and Santa Isabel formations [26–29]. Andesitic lavas and welded ignimbrites from dacitic to a rhyolitic composition rich in plagioclase, biotite, and quartz crystals predominate in the area [30] (Figure 1c). This section of the road presents cutting slopes with large-scale columnar cooling joints with inclinations in the range of  $80^\circ$ – $90^\circ$  and variable heights between 10 m–100 m. This, added to the notorious presence of discontinuities and fallen rock blocks on the road, makes it difficult to collect information in the field and makes it necessary to use remote techniques such as SfM to complement, guarantee, and improve the accuracy of the field information.

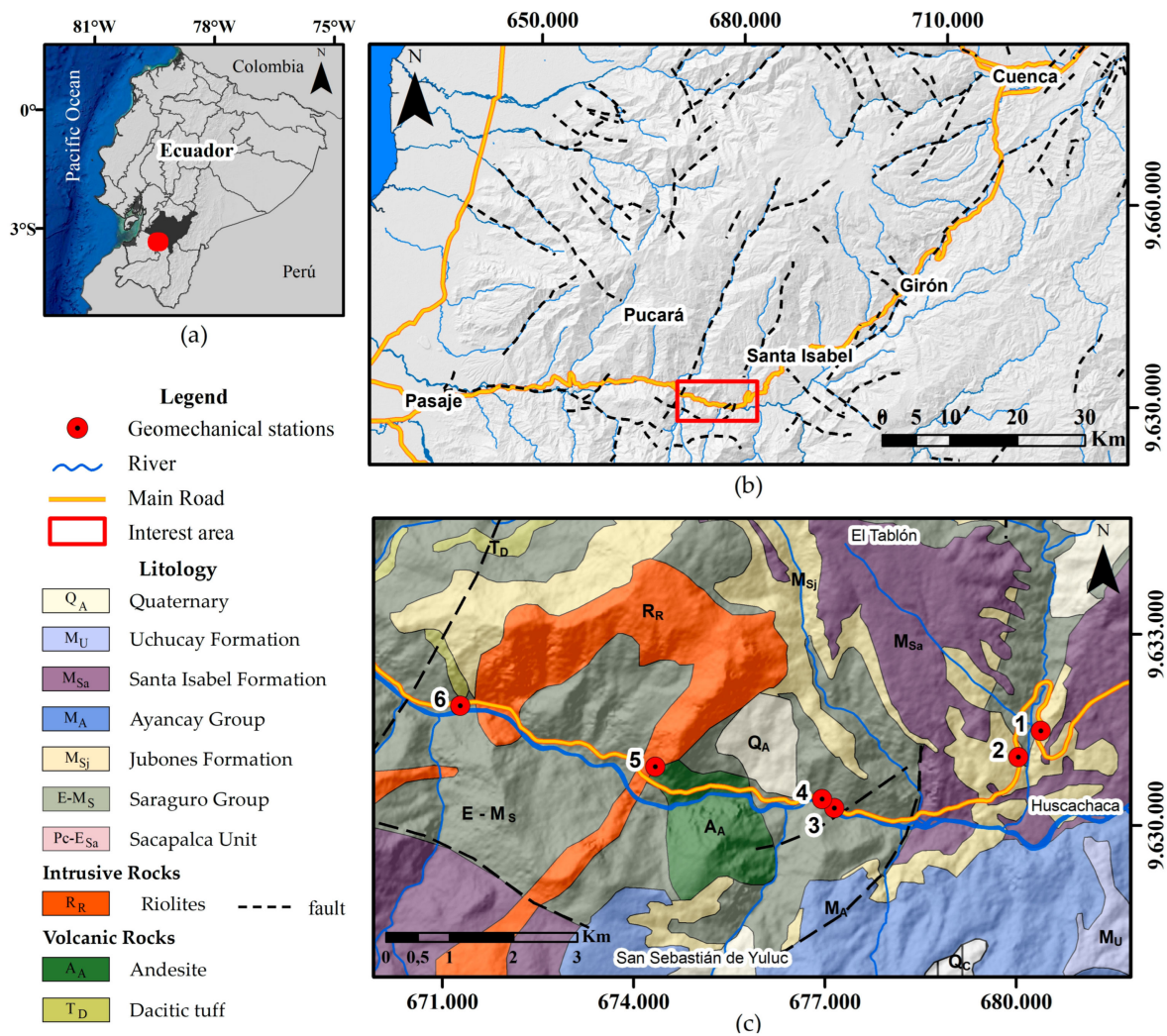


**Figure 1.** General aspects of the study area: (a) Location of the study area: Azuay (Ecuador). (b) Aerial view of the analyzed area with the main structural lineament [31]. (c) Geological map of the study area: Saraguro group ( $E_3n_1S$ ), Jubones formation ( $n_1n_2Jb$ ), Jubones formation ( $n_1n_2Jb$ ). IIGE (2005—modified). The numbers included in the figure are the studied slopes.

## 2. Materials and Methods

### 2.1. Information Gathered in the Field

Generally, information gathering is carried out in the field using geomechanical stations through standardized surveys [1]. However, in this work, remote techniques such as SfM [32,33] were applied to characterize rock masses more safely and quickly, using them to complement the traditional method.

The field campaigns were carried out in May and June 2022. On each slope (Figure 2), nine discontinuity orientation measurements were obtained (dip and dip direction), which later allowed verifying the degree of precision of the photogrammetry. In addition, different characteristics of the discontinuities of the slopes were obtained in the field, such as roughness, degree of weathering, resistance to compression, and quality of the rock, as well as geometric characteristics of the slope, such as height, orientation, and type. Table 1 shows these results. The coordinates are represented in the UTM WGS 84 17S system.

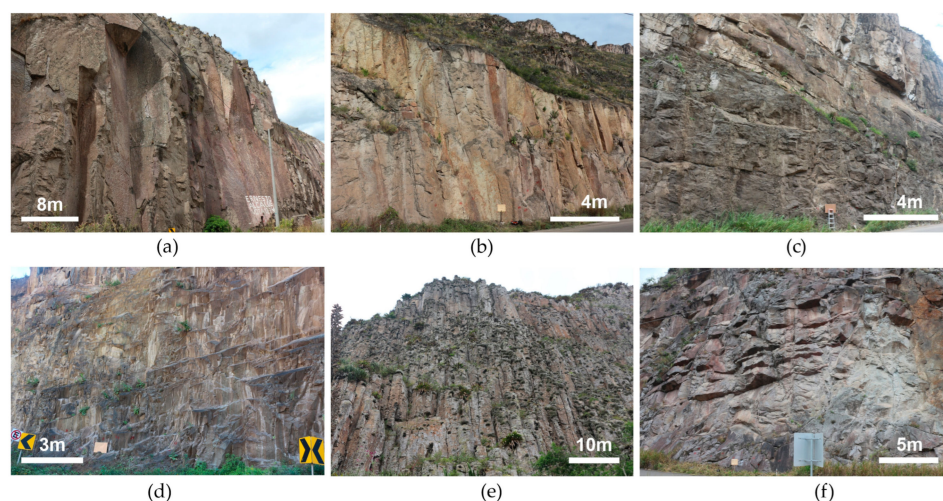


**Figure 2.** General view of slopes analyzed in the Cuenca–Girón–Pasaje route direction East–West: (a) Slope 1; (b) Slope 2; (c) Slope 3; (d) Slope 4; (e) Slope 5; (f) Slope 6.

**Table 1.** General information on the location, geometry, and orientation of the analyzed slopes (dip direction and dip of slopes are indicated, not joint sets).

Slope N <sup>o</sup>	Location	Coordinates		Height (m)	DIP Slope (°)	DIP DIR Slope (°)	Type of Slope	No. of Photographs
		East	North					
1	km 78 + 740	680,392	9,631,487	46.80	76	315	Excavated	250
2	km 80 + 900	680,041	9,631,075	13.50	85	55	Excavated	135
3	km 84 + 475	677,153	9,630,275	32.50	82	215	Excavated	82
4	km 84 + 635	676,963	9,630,415	23.60	80	185	Excavated	88
5	km 87 + 700	674,342	9,630,924	40.00	90	45	Natural	109
6	km 91 + 080	671,281	9,631,878	33.70	83	180	Excavated	171

Likewise, a photographic survey was carried out with a Can-non-Eos Rebel T4i digital camera, which allowed complementing the information from the analysis of discontinuities by creating the 3D point cloud. On a board at the foot of the slope aligned vertically (90°), whose course is known, three ground control points are placed with which the 3DPC could be scaled and oriented according to the methodology of [22].

Actually, to generate a digital model of the slope for compass orientation measurements, based on this “fast and low cost” methodology, the type of camera to use is not significant. If it is pursued to elaborate detailed photogrammetry, of course, the better the optics and the sensor, the better the result will be. Until relatively recently, about ten years, calibrated cameras were used for photogrammetry (1). Currently, and for this type of scope, any digital or mobile camera can be used for the objectives pursued in this research. In the case of very large slopes of more than 30 m, the use of a tripod and optical zoom is highly recommended.

## 2.2. 3D Point Cloud

Digital image processing was performed with Agisoft Metashape Version 1.7.3 Demo mode software, which allows 3D construction from multiple views of images. The number of photographs used in these models varies between 82 and 250 (last column of Table 1); photo size 5184 × 3456 pixels; 72 dpi resolution. Quality is greater than 0.5 units, according to [34]. This value is automatically calculated based on the sharpness level of the most focused part of the image.

The processing of the images with Metashape followed these steps [34]: (a) image loading; (b) inspection and discard of images with quality lower than 0.50 units; (c) automatic camera alignment; (d) construction of the 3D point cloud. In each step, we worked

with the highest quality to obtain the greatest number of points and clouds as real as possible (Figure 3a). Then, in the Cloud Compare software version 2.12 [35], the 3DPC obtained was loaded. Finally, using a Brunton-type compass, it was verified that the orientations measured at the points marked (Figure 3b) were similar and consistent compared to the measurements; this was to guarantee that the orientation and scaling of the 3DPC were correct.

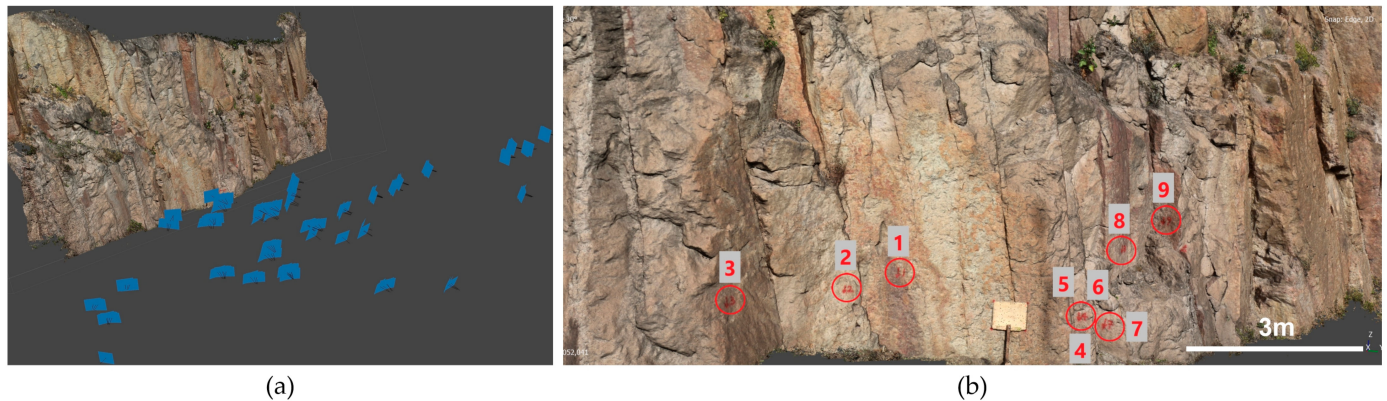


**Figure 3.** Construction of the 3D point cloud with the Agisoft program (for example, Slope 2 located at km 80 + 900): (a) 3D point cloud and camera orientation; (b) orientation control points and ground control points.

### 2.3. Identification of Discontinuities

Once the orientations and scaling of the 3DPC were built and validated, the identification of the discontinuities was carried out using two methods: (a) manual, with the support of the virtual compass of the Cloud Compare software, and (b) automatic, with the open-source program Discontinuity Set Extractor (DSE).

Hundreds of orientation measurements of the discontinuities were obtained manually, according to Table 1, creating groups of points through stereograms. Each important set of points corresponds to a family of discontinuities. On the other hand, DSE is a program that works in the MATLAB environment and allows families of discontinuities and their orientations to be identified automatically [17] (Figure 4). In addition, it is possible to calculate the normal spacing of the discontinuities [20] and the persistence [21]. Table 2 shows the parameters used in the development of this study for the analysis of discontinuities with DSE, in agreement with [17].

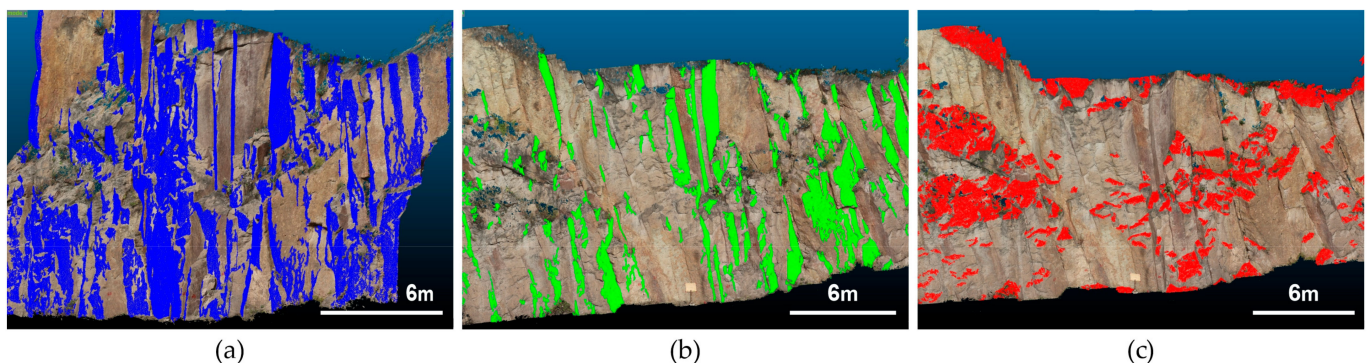


**Figure 4.** Discontinuities automatically identified with DSE of Slope 2 located at km 80 + 900: (a) J1; (b) J2 and (c) J3.

**Table 2.** Parameters used in DSE to obtain discontinuities automatically.

Basis	Parameter	Value
Calculation of the normal vector	The number of closest neighbors (knn).	30
	Tolerance/Coplanarity test (h).	0%
Calculation of the main poles	The number of bins for density analysis.	256
	The minimum angle between the main poles.	30
Assignment of points to main poles	The maximum angle between a pole and its corresponding main pole.	30
	The minimum number of points per Cluster.	100
Cluster Analysis	Cluster plane grouping (k).	2

The parameter that has the greatest influence on the results is the number of neighbors (knn); as knn increases, the calculated normal vectors are less dispersed around the mean value, which means a higher precision is obtained. In the present study, the value of 30, recommended by [17], was adopted. On the other hand, by changing the values of other parameters, possible unrepresentative families of discontinuities can be obtained, thus decreasing the precision and coverage of the main identified discontinuity planes. Very high values of the maximum angle between a pole and its corresponding main pole can give poor results if two families of discontinuities have close orientations, while very low values generate a large number of families of discontinuities that cover most of the studied surface. When applying the minimum number of points per Cluster, values below 100 are recommended, thus eliminating planes that may represent fallen rocks or slope vegetation. While values greater than 100 can eliminate real discontinuity planes.

#### 2.4. Analysis with Empirical Methods

Rock mass classification systems have been used for several decades to assess the behavior of rock-cut slopes [36,37]. The main factors involved in most empirical classifications, according to [38], are the following: (a) intact rock strength (UCS); (b) the quality of the rock (RQD); (c) the conditions of the discontinuities (number of families, roughness, weathering or alteration, spacing and persistence of the discontinuities); (d) groundwater flows; (e) stress-reducing factor (SRF).

The geological strength index (GSI) and the intact rock strength (UCS) were obtained directly in the field through observation and the N-type Schmidt hammer, respectively. At the same time, the RQD and the RMR classification were determined in the office by combining the data obtained in the field and through the 3DPC.

Among the various slope classifications that exist today [39–43], two stand out and are used worldwide: (a) the Slope Mass Rating or SMR [8], which was developed from Bieniawski's RMR, providing adjustment or correction factors (Equation (1)) depending on the type of excavation method (F4) and the orientations of the discontinuities and the slope (F1, F2, F3); (b) the  $Q_{\text{slope}}$  index [7,23], uses the same four parameters RQD,  $J_n$ ,  $J_r$ ,  $J_a$ , of the Barton's Q index and the other two are replaced by the environmental and geological condition number ( $J_{\text{wice}}$ ) and by the greatest of the following stress-reduction factors for the slope considering the physical condition ( $\text{SRF}_a$ ), similar to the Q index ( $\text{SRF}_b$ ), and ( $\text{SRF}_c$ ) that considers the largest discontinuity. In addition, in this system, the discontinuity orientation (O) becomes important (Equation (2)).

$$\text{SMR} = \text{RMR} + (\text{F1} \times \text{F2} \times \text{F3}) + \text{F4} \quad (1)$$

$$Q_{\text{slope}} = \frac{\text{RQD}}{J_n} \times \left( \frac{J_r}{J_a} \right)_O \times \frac{J_{\text{wice}}}{\text{SRF}_{\text{slope}}} \quad (2)$$

In [23], a simple formula (Equation (3)) is presented to determine the maximum slope angle that a slope can have to be considered stable and not require support. The said angle is compared to determine if the slope is stable or unstable.

$$\beta = 20 \log_{10} Q_{\text{slope}} + 65^{\circ} \quad (3)$$

Additionally, considering that rockfall is an important hazard in rock slope cuts for roads and the presence of rock blocks on the sides of the analyzed road due to the steep cut angles and notorious fractures of the slopes, a rockfall risk analysis was carried out. According to the RHRS<sub>mod</sub> classification, values in the range of 200–300 correspond to medium rockfall risk, while values in the range of 300–400 correspond to slopes with high rockfall risk, for which corrective action is necessary.

To determine the danger of rockfall, the Rockfall Hazard Classification System (RHRS<sub>mod</sub>) modified by [44] was applied, developed from the one presented by the Oregon State Highway Division [45] described in detail in [9] and exemplified in [46]. In [44], the exponential functions applied for calculating the scores of the RHRS<sub>mod</sub> method are shown. For all the slopes analyzed, the following data were assumed: (a) average vehicle risk (AVR) = 60%; (b) decision sight distance (%D<sub>a</sub>) = 50%; (c) mean annual precipitation (h) = < 400 mm and (d) rockfall frequency (f) = three per year. All other parameters necessary for the methodology were obtained in the field. In addition, it is important to clarify that the fall of individual blocks in the area is typical, so the block size is considered for the score.

### 2.5. Kinematic Analysis

In agreement with [6], and since these are shallow slopes of competent rock with a structurally controlled stability, a kinematic analysis was carried out with the support of DIPS software Version: 6.008 from Rocscience Inc., Toronto, ON, Canada. The families of discontinuities were identified automatically with the DSE program, and the friction angle was determined by applying the criterion of [25]. The kinematic analysis was carried out with DIPS, and it was corroborated with the failure conditions for planar failure, wedge failure, and overturning failure defined by [5], which are a function of the friction angle, dip, and direction of dip of both the discontinuities and the slope.

For applying the Barton & Bandis criterion, the following parameters were assumed: basic friction angle  $\phi_b = 35^{\circ}$ , rock specific weight  $\gamma = 0.026$  MPa, and joint roughness coefficient JRC = 8 for all the slopes. The compressive strength of the JCS joints was measured in the field with the Schmidt hammer, and  $\phi_r$  was obtained according to what is indicated in the Barton—Choubey relation [47], ranging from 26 grades to 31 grades.

### 2.6. Limit Equilibrium Analysis

The types of slope failure can be: (a) circular [2], (b) demolition [2], (c) planar [3], and (d) wedge [4]. The first two types of failure require knowing the geometry in detail; hence, as the objective of this study is to use low-cost methodologies, it became impossible to carry out a limit equilibrium analysis of the slopes for these types of failure. However, a limit equilibrium analysis, also known as an analytical analysis, was carried out by determining the Factor of Safety (FS) (Equation (4)) for plane and wedge breaks. The analytical analysis calculates the resistant or stabilizing forces ( $F_{\text{est}}$ ) and divides them by the acting or destabilizing forces ( $F_{\text{des}}$ ), obtaining a value greater than 1 to consider that the slope is stable.

$$FS = \frac{F_{\text{est}}}{F_{\text{des}}} \quad (4)$$

The stability analysis of the slopes for flat failures was carried out with the help of the commercial program RocPlane Version 2.029, which analyzes the stability of flat landslides using the limit equilibrium method. On the other hand, the Swedge Version 4.078 program was used for the wedge failure analysis, which evaluates the geometry and stability of tetrahedral surface wedges in rocky slopes using limit equilibrium methods. The calculation of the stabilizing forces in the case of plane cracks was applied using the Barton & Bandis criterion (Equation (5)), with the same parameters calculated in the

kinematic analysis. While for the analysis of wedge failures, the Mohr–Coulomb criterion was applied, assuming zero cohesion, the most unfavorable condition of the slope.

$$\tau = \sigma_n \tan \left[ \text{JRC} \log_{10} \left( \frac{\text{JCS}}{\sigma_n} \right) + \phi_r \right] \quad (5)$$

### 3. Results

#### 3.1. Analysis of Families of Discontinuities

From the point clouds obtained for each of the slopes and explained in detail in Section 2, it was possible to identify between three and four families of discontinuities ( $J_i$ ) using the two applied techniques. For the manual analysis, between 150 and 300 planes were measured. On slope number 5, the manual analysis identified a fourth family of discontinuities ( $J_4$ ), which has a dip close to zero and does not outcrop, so it is not found in the automatic analysis. The automatic analysis with DSE allows the measurement of thousands and even millions of points, identifying important discontinuities not defined in the manual analysis, as in the case of Slopes 1 and 6. Table 3 presents the families of discontinuities obtained by the two methods and the number of measurements in each analysis.

**Table 3.** Orientations of the discontinuities obtained manually by combining the measurements with a compass in the field and a virtual compass, and those obtained automatically with DSE (note that in the table, the orientation of joint set is referred to as dipdirection/dip).

Slope N°	Virtual Analysis					Number of Measurements	Automatic Analysis				DSE Measurements (Pts */Cluster)
	Joint Sets Identified (Orientation DipDir/Dip)				Joint Sets Identified (Orientation DipDir/Dip)						
	J1	J2	J3	J4		J1	J2	J3	J4		
1	315/75	274/81	051/86	N.I.	190	319/76	276/80	055/88	156/34	3,586,666 */684	
2	067/83	012/81	050/51	N.E.	250	070/86	015/80	073/39	N.E.	754,110 */442	
3	222/88	166/30	184/89	025/46	300	216/83	189/39	000/85	057/72	1,941,850 */1136	
4	011/76	206/36	185/82	055/82	151	355/75	204/45	193/75	036/76	447,726 */784	
5	269/89	233/86	160/89	347/03	186	261/87	230/87	170/89	N.I.	481,677 */342	
6	174/68	340/37	N.I.	327/84	230	183/68	337/39	216/86	326/85	1,542,583 */1374	

N.I. = Not Identified; N.E. = Does not exist; \* Number of orientation measurements found automatically.

The dip and dip direction values presented in Table 1 refer to the orientation of the analyzed slope. On the other hand, Table 3 presents the orientations of the different families of discontinuities identified from the 3D point cloud (3DPC) for the two analyses. The manual analysis was carried out in the Cloud Compare program through the virtual compass, while the automatic analysis was carried out with the Discontinuity Set Extractor (DSE) program. As mentioned in the discussion, the mean absolute variation of dip direction and dip is less than 10° and 5°, respectively, between the orientations obtained manually with Cloud Compare and those obtained automatically with DSE. The average precision of the dip direction is 4 degrees, and the dip is 2 degrees, with a maximum variability of 6 degrees in the dip direction for one of the slopes studied. This comparison corresponds to the measurement of the 9 field control planes of each slope (Figure 3b) with those obtained with the virtual compass from the 3DPC, at the same marked points. This procedure was carried out in order to verify and guarantee that the orientation and scaling of the 3DPC are adequate.

Table 3 shows the measurements of each joint set identified: Virtual Analysis indicates that this joint set has been identified in the CloudCompare program (the set notation is the same as those identified in the field at geomechanical stations) and its dip direction and dip (orientation) has been measured using the program's "measure compass" tool. The block on the right of Table 3 refers to the automatic measurement of joint sets: using the same CloudCompare model already analyzed, an automatic measurement of joints is performed with the DSE application. The results are not the same as obtained manually,

since a multitude of planes is measured that are grouped into sets and do not have to be the same planes measured. Note, for example, in Table 3, slope J1, that in Virtual Analysis, 190 measurements have been made, and in Automatic, more than three million. On the other hand, the “precision” of the methodology, combining manual and remote, has been carried out with the so-called “control planes”, which, as mentioned, there are nine, and they simply consist of marking a plane with a color and measuring it accordingly—manually and then in the CloudCompare program.

For the analysis in which it is necessary to know the orientation of the discontinuities, as is the case of the kinematic analysis and SMR, we worked with those identified automatically since it eliminates the subjectivity of the authors. Figure 5 shows the discontinuities obtained for each slope with the support of the DSE program.

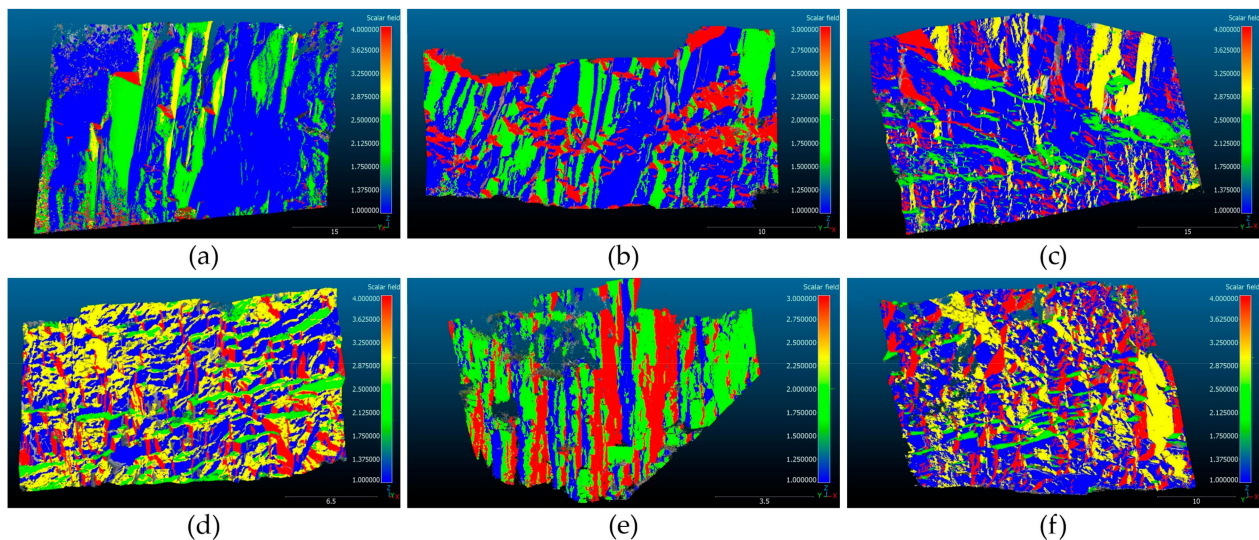


**Figure 5.** Automatic identification of discontinuities with the support of the DSE program: (a) Slope 1; (b) Slope 2; (c) Slope 3; (d) Slope 4; (e) Slope 5; (f) Slope 6.

### 3.2. Rock Mass Classification Systems

#### 3.2.1. Slope Mass Rating

According to the basic RMR, the rock masses are of fair to good quality with values between 50 and 70; however, when applying the correction factors to determine the SMR, values below 40 were obtained in five of the six slopes analyzed, classifying them as poor-quality unstable slopes. The orientation of the most unfavorable discontinuities could cause a wedge failure on Slopes 1 and 6 and a possible planar failure on Slopes 2, 3, and 4. It is also worth mentioning that four of the slopes analyzed are partially stable against failure due to overturning. Table 4 shows the results, parameters, and factors considered to obtain the SMR.

**Table 4.** Parameters and correction factors used to determine the SMR rock mass classification system for slopes.

Slope N°	GSI	RQD	UCS (MPa)	RMR	Break (Family)	Correction Factors				SMR	Stability
						F1	F2	F3	F4		
1	75–80	100	40	70	P (J1)	1.00	1.00	−25		45	PS
					W (J2–J3)	0.70	1.00	−50	0	35	U
					T (J3)	0.40	1.00	−6		67	S
2	60–65	95–100	38	60	P (J3)	0.70	0.85	−60		24	U
					W (J1–J2)	0.15	1.00	−50	0	52	PS
					T	0.15	1.00	0		60	S
3	55–60	85–95	40	59	P (J2)	0.40	0.85	−60		38	U
					W (J2–J4)	0.15	0.40	−60	0	55	PS
					T (J4)	0.40	1.00	−25		49	PS
4	55–60	77–87	51	63	P (J2)	0.70	0.85	−60		27	U
					W (J3–J4)	0.15	0.85	−60	0	55	PS
					T (J1)	0.70	1.00	−25		45	PS
5	50–55	75–85	58	53	P	0.15	0.15	0		68	S
					W	0.15	0.15	0	15	68	S
					T (J2)	0.85	1.00	−25		46	PS
6	50–55	50–60	46	46	P (J1)	1.00	1.00	−60		10	U
					W (J1–J4)	0.15	1.00	−60	0	37	U
					T (J4)	0.15	1.00	−25		42	PS

P = planar tear; W = wedge break; T = Overturning; U = unstable; PS = partially stable; S = stable.

### 3.2.2. $Q_{\text{slope}}$ Index

All the slopes analyzed are formed by competent rocks and are located in a desert environment. In general, the slopes present a degree of alteration with small displacements and roughness between smooth flat and rough wavy. According to the  $Q_{\text{slope}}$ , Slope 1 can be considered stable. While in the other slopes, all present dip angles were much greater than the one suggested ( $\beta$ ) by this classification method (Table 5). The  $Q_{\text{slope}}$  classification was created to analyze highway slopes, which is why on Slope 5, a natural slope, the results are inconsistent when compared to the SMR classification.

**Table 5.** Calculation of the average parameters to identify the  $Q_{\text{slope}}$  of the slopes studied: U = unstable; S = stable.

Slope N°	RQD	Calculation Factors					$Q_{\text{slope}}$	$\beta$ (°)	Stability	
		Jn	Jr	Ja	Ofactor	Jwice				SRF
1	100	9	3	4	1.00	1	2.5	3.33	75	S
2	100	9	2	6	0.75	0.8	5	0.44	58	U
3	90	15	3	2	0.75	0.8	5	1.08	66	U
4	80	15	3	2	0.75	0.8	5	0.96	65	U
5	80	9	1	6	0.50	0.8	4	0.15	48	U
6	55	9	3	4	0.50	0.8	5	0.37	56	U

When carrying out the SMR classification, the F4 correction factor is considered, which depends on the type of slope excavation, and in the case of being a natural slope, 15 points are assigned to it since it has not been subjected to any type of external actions. In addition to this, SMR considers the orientations of the discontinuities and the slope to calculate the other correction factors that allow the SMR value to be determined; on the other hand, the  $Q_{\text{slope}}$  system does not consider whether the slope is excavated or natural in any of its parameters.

### 3.2.3. Modified Rockfall Rating System (RHRS<sub>mod</sub>)

The notorious presence of fallen rocks arranged on one side of the analyzed road makes the classification through this method more critical. On this occasion, the modified RHRS system was preferred over the traditional Hoek system because the methodology proposed by [44] adds the previously calculated Slope Mass Rating (SMR) category to the scoring evaluation. The RHRS<sub>mod</sub> classification was not applied to Slope 5 since it is not a road slope. RHRS<sub>mod</sub> values of 368, 240, 281, 240, and 344 were obtained for Slopes 1, 2, 3, 4, and 6, respectively. These values correspond to medium to high rockfall risks that require corrective measures. Table 6 shows the parameters applied with the score adopted in the analyzed slopes.

**Table 6.** Values and scores for each of the parameters applying the RHRS<sub>mod</sub> methodology.

Category	Slope 1		Slope 2		Slope 3		Slope 4		Slope 6	
	Value	Point								
Slope height (H) meters	46.8	81	13.5	7	32.5	81	23.6	32	33.7	81
Trench Effectiveness	N.c.	81								
Average Vehicle Risk (AVR)	60	14	60	14	60	14	60	14	60	14
Decision sight distance (%Da)	50	47	50	47	50	47	50	47	50	47
Road width (Lc) meters	10	25	10	25	10	25	10	25	10	25
Slope Mass Rating (SMR)	27	26	24	39	38	10	27	26	10	81
Block size (Db)	2.86	81	0.72	14	0.63	10	0.22	2	0.27	3
Annual rainfall (h) mm/year	400	4	400	4	400	4	400	4	400	4
Rockfall frequency (f)	3	9	3	9	3	9	3	9	3	9

In Slope 5, it is not possible to perform the modified rockfall classification (RHRS<sub>mod</sub>) because it is not located on the side of the road, and therefore it cannot be assigned values and scores for different parameters such as: Effectiveness of the ditch, average vehicle risk, decision sight distance, and roadway width. In summary, the classification (RHRS<sub>mod</sub>) cannot be carried out because it is a slope that is not on the side of the road. (RHRS<sub>mod</sub>).

### 3.3. Kinematic Analysis

As shown in Table 7 and Figure 6, different possible failure modes have been identified for five of the six slopes analyzed using the kinematic analysis. Four of the slopes studied may present wedge failure, three might have a planar fracture, and two could present failure due to overturning. Slopes 2, 4, and 6 show more than one possible failure mode through kinematic analysis. On the other hand, Slope 3 is identified as partially stable for the three types of failure; however, later, by comparing the results of the other methods, the most probable type of failure will be identified in each slope. The kinematic analysis was carried out on Slope 5 (See Figure 6e and Table 7). According to the SMR classification and the kinematic analysis, it was determined that the instability of Slope 5 could be caused by the J2 family and produce a failure only due to toppling; for this reason, the limit equilibrium analysis was not carried out on said slope.

### 3.4. Limit Equilibrium Analysis

As expected, being consistent with the previous findings obtained, the limit equilibrium analysis presents results of  $FS < 1$ , showing instability for at least one type of failure in each of the slopes studied. However, as shown in Table 8, although in the previous analyses, there was the possibility of a flat and wedge failure for Slopes 2 and 4, respectively, with this analysis, it is observed that for them, in some cases, Factors of Safety are greater than one ( $FS > 1$ ), thus determining that these types of failures are not the most unfavorable for the said slopes. In the slopes in which, through the SMR classification and kinematic analysis, it was determined that the possible failure was due to toppling, the limit equilibrium analysis was not carried out because there was no detailed geometry of the slopes.

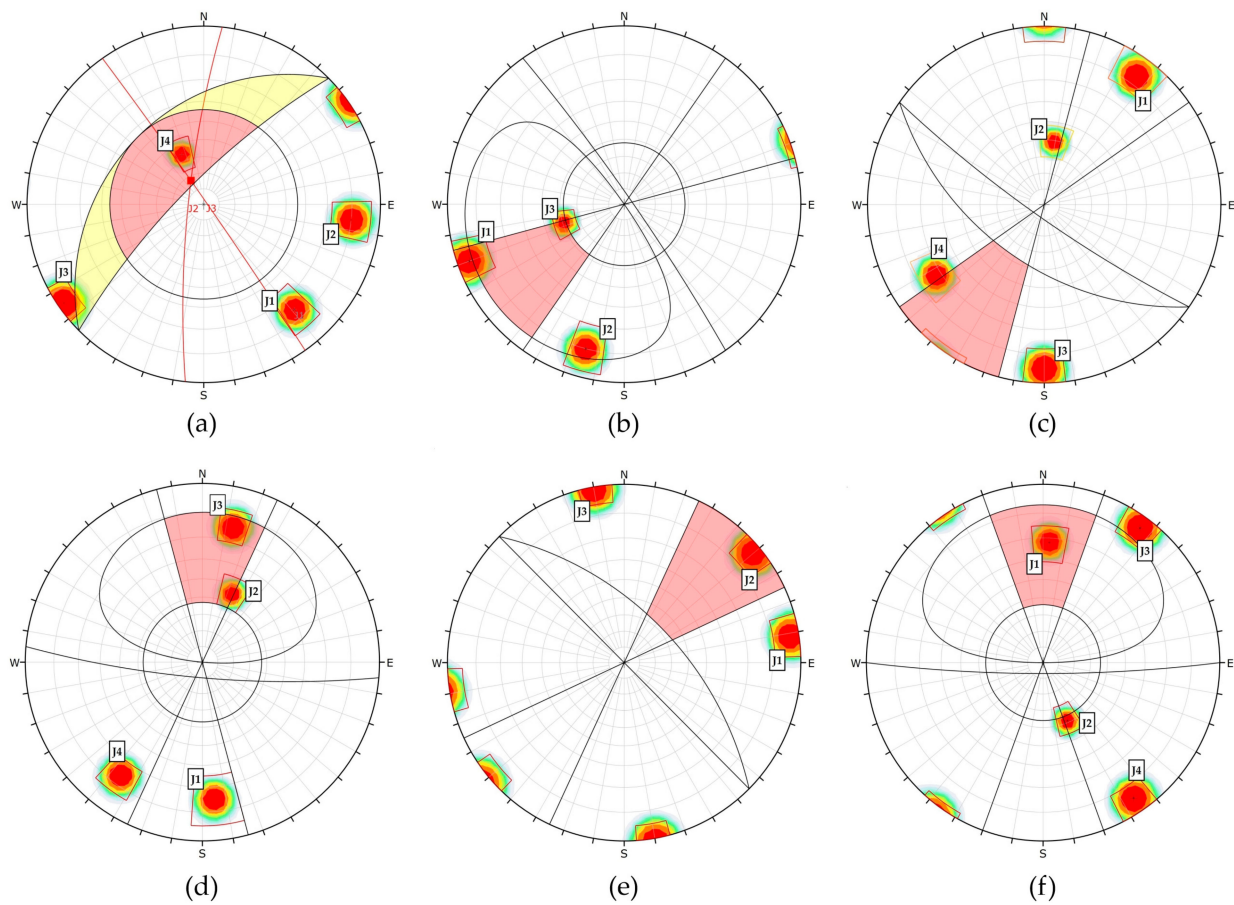


**Figure 6.** Kinematic analysis: (a) Slope 1 (possible wedge failure J2–J3); (b) Slope 2 (possible planar failure by J3); (c) Slope 3 (possible overturning J4); (d) Slope 4 (possible planar fracture J2 and J3); (e) Slope 5 (possible overturning J2); (f) Slope 6 (possible planar failure J1).

**Table 7.** Kinematic analysis: parameters and results to determine the stability of the slopes studied: P = planar; W = wedge; T = Overturning; U = unstable; S = stable.

Slope N°	$\phi_i$ (°)	Type of Break	Stability	Discontinuity to Consider
1	34	P	S	/
		W	U	J2–J3
		T	S	/
2	38	P	U	J3
		W	U	J1–J2
		T	S	/
3	29	P	PS	J2
		W	PS	J2–J4
		T	PS	J4
4	37	P	U	J2 y J3
		W	U	J3–J4
		T	U	J1
5	32	P	S	/
		W	S	/
		T	U	J2
6	36	P	U	J1
		W	U	J1–J4
		T	PS	J2

**Table 8.** Limit Equilibrium Analysis: safety factor against most unfavorable discontinuities: W = Wedge; P = Planar.

Slope N°	Type of Failure	Security Factor (FS)	Discontinuity to Consider
1	W	0.56	J2–J3
2	P	1.31	J3
	W	0.14	J1–J2
3	P	0.96	J2
	W	0.68	J2–J4
4	P	0.39	J3
	W	0.10	J3–J4
6	P	0.47	J1
	W	0.29	J1–J4

#### 4. Discussion

The acquisition of the photographs, the measurement of the control points using a manual compass and a tape measure, and the analysis of the opening, roughness, resistance, and weathering of the discontinuities were the works carried out in the field. With the application of the SfM technique and the creation of the 3DPC in the office, it was possible to identify and measure discontinuities quickly and easily. In addition, the calculation of the spacing and persistence of the discontinuities was performed more safely and accurately. The authors' subjectivity and judgments when manually identifying discontinuities are eliminated when performing an automatic discontinuity analysis with the support of programs such as DSE, thus obtaining more accurate measurements. However, it is important to emphasize that the mean absolute variation of the dip and dip direction are less than 10° and 5°, respectively, between the orientations obtained with the virtual compass and automatically.

Significant fractures and discontinuities are observed on the faces of the six slopes studied, slope dip angles greater than 75°, and heights of several tens of meters. Therefore, it was presumable that possible breaks would be determined and identified when performing the stability analysis. Each method used applies different parameters and considerations; however, in all cases, at least one failure mode was determined for each slope.

From the analyses carried out on Slope 1, a possible wedge failure caused by the intersection of the groups of discontinuities J2–J3 was determined. Slope 1 has the smallest dip angle of the slopes studied and an RQD = 100, so it would be expected that a large part of the slope was considered stable, as established by the  $Q_{\text{slope}}$  classification. However, in Figure 1a, in the upper left part, the wedge-type failure of the slope was clearly observed. In the case of Slope 2, located at km 80 + 900, its instability was identified by all the methods analyzed. The intersection of the J1–J2 discontinuities could cause a wedge-type failure, which would be the expected failure plane; however, no failure has yet been observed in the field, and visually it was considered a stable slope. For Slope 3, two possible failure modes were determined: the first planar failure produced by J2 and the second planar failure produced by the intersection of J2–J4. Visually, some wedge and planar cracks were observed, consistent with what was established in the analyses. Slope 4 is a quite particular case since, according to the SMR classification and the kinematic analysis, they determined the possibility that the three types of failure, while the limit equilibrium analysis confirms the possible planar failure caused by J3 and the wedge generated by the intersection of J3–J4; while in the field observation, no type of failure or breakage has yet been observed. In Slope 5, the possible failure due to overturning was determined only by means of the kinematic analysis, while according to the SMR, it was considered stable as it is a natural slope; on the other hand, small fallen blocks were visually observed, but with large openings between the discontinuities, and also quite loose and large blocks. As for Slope 6, located at km 91 + 080, both visually and through analysis, planar breaks caused by J1 and wedge breaks were identified due to the intersection of discontinuities J1–J4.

On the other hand, the  $RHRS_{mod}$  classification becomes essential due to the large number of rocks of considerable size arranged on the sides of the road. In the slopes analyzed,  $RHRS_{mod}$  values greater than 300 are found in Slopes 1 and 3, which require immediate corrective measures. Additionally, it would be important to focus future studies on the area solely on the  $RHRS_{mod}$  classification since there are a large number of high- and poor-quality slopes there, prone to constant landslides and rockfalls.

This study highlights the importance of using several slope stability analysis methods, which allow for comparing and adequately identifying their stability and the failure mode, and the discontinuities to be considered. However, it is imperative to identify the most appropriate analysis methods according to the reality of each slope. For example, the  $Q_{slope}$  classification was created for the excavation of new slopes, so in this study, it does not provide the same amount of information compared to the SMR, kinematic, and limit equilibrium. In addition, it can give false results, as in the case of the present Slope 1 in which a wedge fracture was clearly observed; however, by means of  $Q_{slope}$  it was determined as stable.

Finally, in Table 9, a summary of the stability of the slopes studied is presented, determined by the methods mentioned above, and a comparison is made with what was observed in the field.

**Table 9.** Identification of the stability of the slopes studied by the different methods: U = Unstable; S = Stable; N.A. = Not Applicable; M = Medium Risk; H = High Risk.

Slope N°	SMR	$Q_{slope}$	$RHRS_{mod}$	Kinematic	Analytic	Visual	Description
1	U	S	H	U	U	U	Wedge cracks
2	U	U	M	U	U	S	No breakage observed
3	U	U	M	S	U	U	Planar and wedge cracks
4	U	U	M	U	U	S	No breakage observed
5	S	N.A.	N.A.	U	N.A.	U	Very loose blocks/overturning observed
6	U	U	H	U	U	U	Planar and wedge cracks

## 5. Conclusions

The methodology followed in the present work for the use of the SfM technique allowed the survey of the slopes in a safe and fast way, acquiring the photographs with the respective control points in an average time of 20 min per slope. SfM allows a detailed analysis of the discontinuities in terms of orientation, spacing, and persistence and provides unbeatable access capacity to elevated areas on high slopes. From the photographs, it was possible to reconstruct the slope and identify the discontinuities with DSE automatically with the measurement of thousands of orientations from the 3DPC, thus eliminating subjectivity and the low amount of data obtained with the virtual compass in Cloud Compare; however, maintaining consistency in the results obtained in both cases.

In the five different methodologies used to analyze the stability of the slopes, results attached to reality were obtained. When applying the  $Q_{slope}$ , whose methodology does not consider the orientation of the discontinuities, findings can differ from what is observed in reality, as is the case of Slope 1, which was determined stable, even though a detachment of a block of considerable size was clearly noticed. On the other hand, the SMR classification system is ideal for the study area since it considers the type of excavation and the orientation of the discontinuities, which must be complemented with a kinematic analysis for possible planar, wedge, and overturning fractures; or with a limit equilibrium analysis for planar and wedge fractures to validate the results. In addition, SMR is a necessary parameter for the  $RHRS_{mod}$  classification implemented in the present study.

Incorporating detailed information on the parameters involved in the  $RHRS_{mod}$  classification will allow more realistic results and an in-depth analysis of different slopes in the study area regarding the danger of falling rocks. In the study area, a large number of fallen rocks are observed on the side of the road, and closures and even road accidents

are common in winter due to rockfalls. Therefore, a call is made to delve into the rockfall hazard classifications to identify high-risk areas of rockfall along the highway and propose possible corrective measures.

**Author Contributions:** Conceptualization, X.D.-R., C.P.-M., S.L., M.D.P.V.E., M.M. and L.J.-B.; methodology, X.D.-R., C.P.-M., S.L., M.D.P.V.E., M.M. and L.J.-B.; software, X.D.-R., C.P.-M. and L.J.-B.; validation, S.L., M.D.P.V.E., M.M. and L.J.-B.; formal analysis, X.D.-R. and C.P.-M.; investigation, X.D.-R., C.P.-M., S.L., M.D.P.V.E., M.M. and L.J.-B.; resources, S.L., M.D.P.V.E., M.M. and L.J.-B.; data curation, X.D.-R., C.P.-M., S.L., M.D.P.V.E., M.M. and L.J.-B.; writing—original draft preparation, X.D.-R. and C.P.-M.; writing—review and editing, X.D.-R., C.P.-M., S.L., M.D.P.V.E., M.M. and L.J.-B.; supervision, S.L., M.M. and L.J.-B.; project administration, M.M. and L.J.-B.; funding acquisition, M.M. All authors have read and agreed to the published version of the manuscript.

**Funding:** This research is partially funded by the Research Deanship of ESPOL Polytechnic University and by the Geotechnics Master Program of the Faculty of Engineering in Earth Sciences (FICT, acronym in Spanish) of ESPOL Polytechnic University in Guayaquil, Ecuador.

**Acknowledgments:** This research is the final product of a master thesis of the Geotechnics Master Program of the Faculty of Engineering in Earth Sciences (FICT, acronym in Spanish) of ESPOL Polytechnic University in Guayaquil, Ecuador. The authors thank the support of the Dean of Research at ESPOL Polytechnic University. Last but not least, we are grateful to the editor and the three anonymous referees for the detailed reviews that helped us improve the manuscript.

**Conflicts of Interest:** The authors declare no conflict of interest.

## Abbreviations

The following Abbreviations were used in the text:

SMR	Slope Mass Classification
RHRS	Rockfall Hazard Classification System
$Q_{\text{slope}}$	Barton's Q slope index
SfM	Structure from Motion
DSE	Discontinuity Set Extractor
RMR	Rock Mass Classification
$Q_{\text{system}}$	Barton's Q index
3DPC	3D Point Cloud
JRC	Joint roughness coefficient
JCS	Joint wall compressive strength
UCS	Intact rock strength
RQD	Rock quality designation
SRF	Stress reduction factor
GSI	Geological resistance index
$J_r$	Joint Roughness number
$J_n$	Joint set number
$J_a$	Joint alteration number
$J_{\text{wice}}$	Environmental and geological condition number
O	Orientation factor of discontinuities
F1-F2-F3	Adjustment to RMR based on orientations
F4	Adjustment to RMR based on excavation method
$\beta$	Maximum slope angle $Q_{\text{slope}}$
$\phi_b$	Basic friction angle
$\phi_r$	Residual friction angle
$\phi_i$	Instantaneous friction angle
$\sigma_n$	Normal effort
$\tau$	Hoop stress
$\gamma$	Specific weight
FS	Security factor
$F_{\text{est}}$	Stabilizing forces
$F_{\text{des}}$	Destabilizing forces

## References

1. Jorda, L.; Tomás, R.; Rodriguez, M.; Abellan, A. *Manual de Estaciones Geomecánicas. Descripción de Macizos Rocosos En Afloramientos*; ETSI Minas: Madrid, Spain, 2016; ISBN 978-84-96140-55-4.
2. Mohtarami, E.; Jafari, A.; Amini, M. Stability Analysis of Slopes against Combined Circular–Toppling Failure. *Int. J. Rock Mech. Min. Sci.* **2014**, *67*, 43–56. [[CrossRef](#)]
3. Johari, A.; Lari, A.M. System Probabilistic Model of Rock Slope Stability Considering Correlated Failure Modes. *Comput. Geotech.* **2017**, *81*, 26–38. [[CrossRef](#)]
4. Deng, D. Limit Equilibrium Analysis on the Stability of Rock Wedges with Linear and Nonlinear Strength Criteria. *Int. J. Rock Mech. Min. Sci.* **2021**, *148*, 104967. [[CrossRef](#)]
5. Zhou, X.; Chen, J.; Chen, Y.; Song, S.; Shi, M.; Zhan, J. Bayesian-Based Probabilistic Kinematic Analysis of Discontinuity-Controlled Rock Slope Instabilities. *Bull. Eng. Geol. Environ.* **2017**, *76*, 1249–1262. [[CrossRef](#)]
6. Jordá-Bordehore, L.; Jordá-Bordehore, R.; Romero-Crespo, P.L. Kinematic Assessment of Multi-Face Round Slopes Using Hemispherical Projection Methods (HPM). *Soils Rocks* **2016**, *39*, 167–176. [[CrossRef](#)]
7. Bar, N.; Barton, N.R. Empirical Slope Design for Hard and Soft Rocks Using Q-Slope. In Proceedings of the 50th US Rock Mechanics/Geomechanics Symposium, Houston, TX, USA, 26–29 June 2016.
8. Romana, M.R. 23—A Geomechanical Classification for Slopes: Slope Mass Rating; Hudson, J.A., Ed.; Pergamon: Oxford, UK, 1993; pp. 575–600. ISBN 978-0-08-042066-0.
9. Bastidas, G.; Soria, O.; Mulas, M.; Loaiza, S.; Jordá-Bordehore, L. Stability Analysis of Lava Tunnels in Santa Cruz Island (Galapagos Islands, Ecuador) Using Rock Mass Classifications: Empirical Approach and Numerical Modeling. *Geosciences* **2022**, *12*, 380. [[CrossRef](#)]
10. Stead, D.; Coggan, J. 13 Numerical Modeling of Rock-Slope Instability. *Landslides Types Mech. Model.* **2012**, *13*, 144–159.
11. Azarafza, M.; Asghari-Kalajahi, E.; Akgün, H. Numerical Modeling of Discontinuous Rock Slopes Utilizing the 3DDGM (Three-Dimensional Discontinuity Geometrical Modeling) Method. *Bull. Eng. Geol. Environ.* **2017**, *76*, 989–1007. [[CrossRef](#)]
12. Riquelme, A.; Cano, M.; Tomás, R.; Abellán, A. Identification of Rock Slope Discontinuity Sets from Laser Scanner and Photogrammetric Point Clouds: A Comparative Analysis. *Procedia Eng.* **2017**, *191*, 838–845. [[CrossRef](#)]
13. Zhang, L. *Engineering Properties of Rocks*; Butterworth-Heinemann: Oxford, UK, 2016; ISBN 0128028769.
14. Westoby, M.J.; Brasington, J.; Glasser, N.F.; Hambrey, M.J.; Reynolds, J.M. ‘Structure-from-Motion’ Photogrammetry: A Low-Cost, Effective Tool for Geoscience Applications. *Geomorphology* **2012**, *179*, 300–314. [[CrossRef](#)]
15. Guo, J.; Wu, L.; Zhang, M.; Liu, S.; Sun, X. Towards Automatic Discontinuity Trace Extraction from Rock Mass Point Cloud without Triangulation. *Int. J. Rock Mech. Min. Sci.* **2018**, *112*, 226–237. [[CrossRef](#)]
16. Li, X.; Chen, Z.; Chen, J.; Zhu, H. Automatic Characterization of Rock Mass Discontinuities Using 3D Point Clouds. *Eng. Geol.* **2019**, *259*, 105131. [[CrossRef](#)]
17. Riquelme, A.J.; Abellán, A.; Tomás, R.; Jaboyedoff, M. A New Approach for Semi-Automatic Rock Mass Joints Recognition from 3D Point Clouds. *Comput. Geosci.* **2014**, *68*, 38–52. [[CrossRef](#)]
18. Riquelme, A.J.; Tomás, R.; Abellán, A. Characterization of Rock Slopes through Slope Mass Rating Using 3D Point Clouds. *Int. J. Rock Mech. Min. Sci.* **2016**, *84*, 165–176. [[CrossRef](#)]
19. Lato, M.J.; Vöge, M. Automated Mapping of Rock Discontinuities in 3D Lidar and Photogrammetry Models. *Int. J. Rock Mech. Min. Sci.* **2012**, *54*, 150–158. [[CrossRef](#)]
20. Riquelme, A.J.; Abellán, A.; Tomás, R. Discontinuity Spacing Analysis in Rock Masses Using 3D Point Clouds. *Eng. Geol.* **2015**, *195*, 185–195. [[CrossRef](#)]
21. Riquelme, A.; Tomás, R.; Cano, M.; Pastor, J.L.; Abellán, A. Automatic Mapping of Discontinuity Persistence on Rock Masses Using 3D Point Clouds. *Rock Mech. Rock Eng.* **2018**, *51*, 3005–3028. [[CrossRef](#)]
22. Bordehore, L.J.; Riquelme, A.; Cano, M.; Tomás, R. Comparing Manual and Remote Sensing Field Discontinuity Collection Used in Kinematic Stability Assessment of Failed Rock Slopes. *Int. J. Rock Mech. Min. Sci.* **2017**, *97*, 24–32. [[CrossRef](#)]
23. Bar, N.; Barton, N. The Q-Slope Method for Rock Slope Engineering. *Rock Mech. Rock Eng.* **2017**, *50*, 3307–3322. [[CrossRef](#)]
24. Saroglou, H.; Marinos, V.; Marinos, P.; Tsiambaos, G. Rockfall Hazard and Risk Assessment: An Example from a High Promontory at the Historical Site of Monemvasia, Greece. *Nat. Hazards Earth Syst. Sci.* **2012**, *12*, 1823–1836. [[CrossRef](#)]
25. Barton, N.; Bandis, S. *Review of Predictive Capabilities of JRC-JCS Model in Engineering Practice*; Elsevier: Amsterdam, The Netherlands, 1990; Volume 182. [[CrossRef](#)]
26. Avilés-Moran, H.; Escobar Segovia, K.; Flor-Jiménez, M.; Mulas, M.; Murillo-Lozano, I.; Villalta-Echevarría, M. Geotechnical and Structural Characterization of the Ignimbritas of the Saraguro Group in the Sector of Santa Isabel-Pucará, Ecuador. In Proceedings of the 17th LACCEI International Multi-Conference for Engineering, Education, and Technology, Montego Bay, Jamaica, 24–26 July 2019.
27. Witt, C. Constraints on the Tectonic Evolution of the North Andean Block Trailing Tail: Evolution of the Gulf of Guayaquil-Tumbes Basin and the Intermontane Basins of the Central Ecuadorian Andes. Ph.D. Thesis, University of Paris 6, Paris, France, 2007.
28. Hungerbühler, D.; Steinmann, M.; Winkler, W.; Seward, D.; Egüez, A.; Peterson, D.E.; Helg, U.; Hammer, C. Neogene Stratigraphy and Andean Geodynamics of Southern Ecuador. *Earth-Science Rev.* **2002**, *57*, 75–124. [[CrossRef](#)]
29. Siravo, G.; Speranza, F.; Mulas, M.; Costanzo-Alvarez, V. Significance of northern Andes terrane extrusion and genesis of the interandean valley: Paleomagnetic evidence from the “Ecuadorian orocline”. *Tectonics* **2021**, *40*, e2020TC0066841997. [[CrossRef](#)]

30. Pratt, W.T.; Figueroa, J.F.; Flores, B.G. *Geology and Mineralization of the Area between 3° and 4° S, Western Cordillera, Ecuador*; British Geological Survey: London, UK, 1997.
31. Villalta Echeverria, M.D.P.; Viña Ortega, A.G.; Larreta, E.; Romero Crespo, P.; Mulas, M. Lineament Extraction from Digital Terrain Derivate Model: A Case Study in the Girón–Santa Isabel Basin, South Ecuador. *Remote Sens.* **2022**, *14*, 5400. [[CrossRef](#)]
32. Kong, D.; Saroglou, C.; Wu, F.; Sha, P.; Li, B. Development and Application of UAV-SfM Photogrammetry for Quantitative Characterization of Rock Mass Discontinuities. *Int. J. Rock Mech. Min. Sci.* **2021**, *141*, 104729. [[CrossRef](#)]
33. Assali, P.; Grussenmeyer, P.; Villemin, T.; Pollet, N.; Viguier, F. Surveying and Modeling of Rock Discontinuities by Terrestrial Laser Scanning and Photogrammetry: Semi-Automatic Approaches for Linear Outcrop Inspection. *J. Struct. Geol.* **2014**, *66*, 102–114. [[CrossRef](#)]
34. Agisoft, L.L.C. *Agisoft PhotoScan User Manual: Professional Edition*; Agisoft LLC: St Petersburg, Russia, 2014.
35. Girardeau-Montaut, D. *CloudCompare*; Fr. EDF R&D Telecom ParisTech: Paris, France, 2016; p. 11.
36. Azarafza, M.; Nikoobakht, S.; Rahnamarad, J.; Asasi, F.; Derakhshani, R. An Empirical Method for Slope Mass Rating–Qslope Correlation for Isfahan Province, Iran. *MethodsX* **2020**, *7*, 101069. [[CrossRef](#)]
37. Siddique, T.; Alam, M.M.; Mondal, M.E.A.; Vishal, V. Slope Mass Rating and Kinematic Analysis of Slopes along the National Highway-58 near Jonk, Rishikesh, India. *J. Rock Mech. Geotech. Eng.* **2015**, *7*, 600–606. [[CrossRef](#)]
38. Pantelidis, L. Rock Slope Stability Assessment through Rock Mass Classification Systems. *Int. J. Rock Mech. Min. Sci.* **2009**, *46*, 315–325. [[CrossRef](#)]
39. Selby, M.J. A Rock Mass Strength Classification for Geomorphic Purposes: With Tests from Antarctica and New Zealand. *Z. Für Geomorphol.* **1980**, 31–51. [[CrossRef](#)]
40. Robertson, A.M. Estimating Weak Rock Strength. In Proceedings of the SME Annual Meeting, Phoenix, AZ, USA, 25–28 January 1988; pp. 1–5.
41. Hack, R. An Evaluation of Slope Stability Classification. In Proceedings of the ISRM International Symposium-EUROCK 2002, Madeira, Portugal, 25–27 November 2002.
42. Tomás, R.; Delgado, J.; Serón, J.B. Modification of Slope Mass Rating (SMR) by Continuous Functions. *Int. J. Rock Mech. Min. Sci.* **2007**, *44*, 1062–1069. [[CrossRef](#)]
43. Mazzoccola, D.F.; Hudson, J.A. A Comprehensive Method of Rock Mass Characterization for Indicating Natural Slope Instability. *Q. J. Eng. Geol. Hydrogeol.* **1996**, *29*, 37–56. [[CrossRef](#)]
44. Budetta, P. Assessment of Rockfall Risk along Roads. *Nat. Hazards Earth Syst. Sci.* **2004**, *4*, 71–81. [[CrossRef](#)]
45. Pierson, L.A.; Davis, S.A.; Van Vickle, R. *Rockfall Hazard Rating System: Implementation Manual*; Report/Paper Numbers: FHWA-OR-EG-90-01; TRB Publications: Washington, DC, USA, 1990.
46. Peševski, I.; Jovanovski, M.; Guy, M.; O’Hare, N. Rockfall Hazard Assessment for Access Road to Dam “Sveta Petka” Using Rockfall Hazard Rating System (RHRS). *Geol. Maced.* **2011**, *25*, 11–20.
47. Barton, N.; Choubey, V. The Shear Strength of Rock Joints in Theory and Practice. *Rock Mech.* **1977**, *10*, 1–54. [[CrossRef](#)]

**Disclaimer/Publisher’s Note:** The statements, opinions and data contained in all publications are solely those of the individual author(s) and contributor(s) and not of MDPI and/or the editor(s). MDPI and/or the editor(s) disclaim responsibility for any injury to people or property resulting from any ideas, methods, instructions or products referred to in the content.